Magnetic field mapping system on the H-1 heliac[a)]

M. G. Shats, D. L. Rudakov, B. D. Blackwell, L. E. Sharp, and O. I. Fedyanin[b)]
Plasma Research Laboratory, Research School of Physical Sciences and Engineering, The Australian National University, Canberra, ACT 0200, Australia

(Presented on 9 May 1994)

The H-1 heliac recently brought into operation is a medium-sized 3-field-period heliac with major radius $R_0=1$ m, plasma mean minor radius $\langle a\rangle \leqslant 0.2$ m and a wide range of rotational transforms $0.6 \leqslant \iota(0) \leqslant 2.0$. Electron beam mapping of the vacuum magnetic field was performed using new type of a fluorescent target (movable fluorescent rod array having a transparency about 98%). Up to 150–200 toroidal transits were observed at each electron gun position. The spatial resolution of the system was about 3 mm. Electron collector probes were used for monitoring the positions of the magnetic surfaces in different toroidal field periods. Visible paths of the electron beam due to the excitation of the background gas ($p\sim10^{-4}$ Torr) were used for identification of the toroidal transit numbers. This newly developed method gives an accuracy in measurement of the rotational transform of about 1.5%. Experimental surfaces and measured ι profiles show very good agreement with the computer model results. © *1995 American Institute of Physics.*

I. INTRODUCTION

Experimental study of the magnetic geometry in stellarator-type machines is essential to confirm *in situ* the existence of nested closed flux surfaces and to search for possible deviations from the intended magnetic structure. All experimental methods use an electron beam launched parallel to the magnetic field and analyze its trajectory as it follows magnetic field lines. Detecting the position of the electron beam in a poloidal cross section of the machine after a number of toroidal transits allows us to define a drift surface that is close to the true flux surface provided the energy of the electrons is sufficiently low. It is essential that the diagnostic system can resolve small (less than $0.05\langle a\rangle$) magnetic islands and to measure a rotational transform during the magnetic mapping. In this paper, we present the electron-beam diagnostic for study of the magnetic field in the recently built H-1 heliac.[1] A new type of the fluorescent target used in this experiment has a high transparency and allows fast image accumulation. This design combines the advantages of a fluorescent mesh and single rod systems. A new method of identification of the toroidal transit number of the electrons is used.

II. MAGNETIC MAPPING SYSTEM

H-1 is a flexible heliac[1] with a major radius of $R_0=1$ m, plasma mean minor radius $\langle a\rangle \leqslant 0.2$ m, $N=3$ field periods and rotational transform on the magnetic axis $0.5<\iota_0<2.36$ toroidal field coils (TFC) spiral with a swing radius $\rho_s=0.22$ m about a toroidally directed central ring conductor [poloidal field coil (PFC)] that creates a poloidal magnetic field. This coil set produces flux surfaces with bean-shaped cross section whose magnetic axes also follow the helix around the PFC. A helical winding wrapped around the PFC with a swing radius $\rho_h=0.095$ m and in phase with TFCs adds flexibility to the heliac configuration allowing the rotational transform to be varied over a wide range.[2]

Experimental apparatus for the magnetic mapping on the H-1 heliac consists of an electron gun, a fluorescent target, and an electron collector probe. These three elements are located in each of the three toroidal periods of the heliac, so that the electron gun is toroidally spaced 120° from both the fluorescent target and the probe. Such an arrangement allows the positions of the magnetic axis and of the magnetic surfaces in all three periods of the H-1 magnetic field to be compared using available diagnostic ports.

The electron gun is similar to that used in the ATF torsatron.[3] The gun consists of a V-shaped filament made of a thoria-coated tungsten wire (0.3-mm diameter) inside a stainless steel housing (5 mm o.d.) with a replaceable aperture diaphragm (0.5–1.5 mm hole diameter). The stainless steel tubing is grounded and a negative bias voltage is applied to the filament (100–400 V). The gun delivers up to 7 mA of electron current with a filament current of 2 A. The estimated extracted electron current is few hundred μA. The electron gun is supported by a 1.2-cm-diameter hollow stainless steel tube. The tube has a 0.5-cm-diameter tip 25 cm long at the end that is to be inserted into the mapping volume to decrease its effect on the transparency of the apparatus (i.e., to decrease an interception of the toroidally circulating electron beam with the tube). The support tube is mounted on a bellows assembly and is vacuum sealed using a standard Teflon O-ring. The gun is accurately positioned by an R-θ drive and can access any point inside the outermost magnetic surface.

The fluorescent target located at $\phi=120°$ cross section is shown in Fig. 1. It consists of a bean-shaped stainless-steel frame enclosing magnetic surfaces with 21 copper wires stretched across the frame. The wires are phosphor-coated (P24 phosphor was deposited with a brush). The target frame is mounted on a Teflon bearing that is attached to the helical winding of the H-1. This design enables the target to be rotated about the center of the PFC within an angular range

[a)]The abstract for this paper appears in the Proceedings of the Tenth Topical Conference on High Temperature Plasma Diagnostics in Part II, Rev. Sci. Instrum. **66**, 467 (1995).
[b)]Plasma Physics Division, General Physics Institute, Moscow, Russian Federation.

Downloaded 19 Aug 2003 to 150.203.2.60. Redistribution subject to AIP license or copyright, see http://ojps.aip.org/rsio/rsicr.jsp

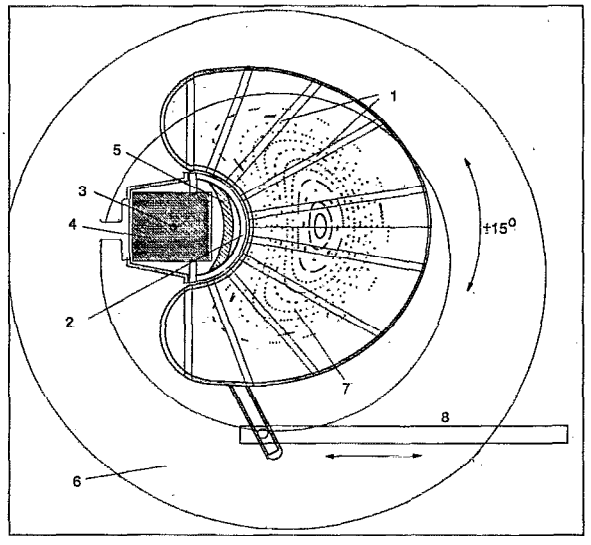

FIG. 1. Schematic diagram of the fluorescent target assembly. (1) Phosphor-coated wires; (2) Teflon bearing; (3) Pivot axes; (4) Poloidal field coil (central ring); (5) Helical winding; (6) Toroidal field coil; (7) Magnetic surfaces; (8) Target drive.

of ±15°. The target is driven through a bellows by a stepping motor located outside the vacuum. When scanned, the wires intersect the poloidal cross section of the magnetic structure almost at right angles to the flux surfaces and cover the entire cross section. The main advantage of this design is that it combines the high transparency ($T=0.98$) of the fluorescent rod systems[4–6] with the larger number of light spots (up to 20 for the outermost surfaces) for each target position and the faster image accumulation of the mesh target.[7,8] All wires are connected in series and are insulated from the target frame and from the construction elements of the machine to enable the measurement of the net electron current to the target. This current is maximized during the alignment of the electron gun to inject the electrons parallel to the magnetic field lines.

Figure 2 presents the arrangement of the fluorescent target and optics in the H-1 vacuum tank. The optical and imaging system consists of a 256×256 pixel CCD camera (EG&G Reticon Camera, type MC9256) with an $f=26$ mm, $f/1.1$ lens, a plane mirror, a negative lens ($f=-100$ mm, $f/1.4$) and a vacuum window. The CCD camera is mounted inside a light-tight reentrant port outside the vacuum, and cooled by compressed air to prevent its overheating. Since the vertical size of the outermost flux surface is expected to be more than 40 cm and the camera is located only about 50 cm away from the fluorescent target, the negative lens is necessary to increase field of view of the camera.

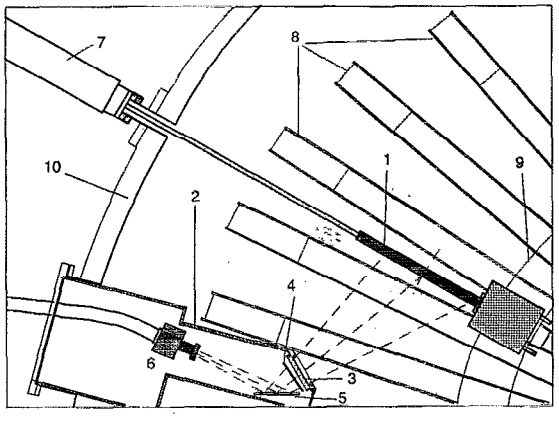

FIG. 2. Arrangement of the fluorescent target and optics in the H-1 heliac. (1) Fluorescent target; (2) Re-entrant port; (3) Vacuum window; (4) Negative lens; (5) Plain mirror; (6) CCD camera; (7) Target drive; (8) Toroidal field coils; (9) Poloidal field coil; (10) H-1 vacuum tank.

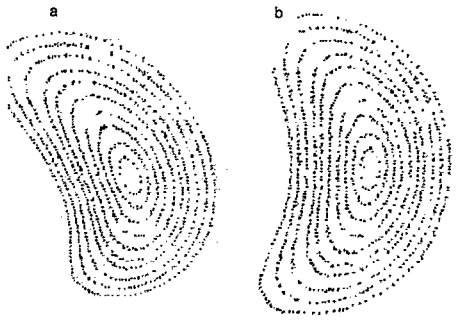

FIG. 3. Measured flux surfaces in the standard magnetic configuration before (a) after (b) geometrical transformation.

III. EXPERIMENTAL PROCEDURE AND SELECTED RESULTS

The digitized images acquired by the CCD camera must be transformed to correct both the perspective distortion and optical aberrations caused mainly by the 10 diopter negative lens. Geometrical transformation of the images is performed by transforming the coordinates (u,v) of the acquired image to the coordinates (x,y) of the corrected image in the form

$$u=\sum_{i=0}^{N}\sum_{j=0}^{N} C_{i,j}x^j y^i, \quad v=\sum_{i=0}^{N}\sum_{j=0}^{N} D_{i,j}x^j y^i, \tag{1}$$

where N is the degree of the polynomial. Polynomial coefficients C_{ij} and D_{ij} are calculated using n known control points. We positioned a ruled grid (size of the grid cell is 2×2 cm) in place of the fluorescent target inside the vacuum tank before the experiment. The image of the ruled grid is used to obtain the (u,v) and (x,y) coordinates of the $n=17$ control points. Calculated coefficients of the second-order polynomials are then applied to the images of the flux surfaces acquired during the magnetic mapping experiment. Figure 3 demonstrates the effect of the geometrical transformation on the shape of the drift surfaces measured in a "standard" magnetic configuration.

The existence of a set of closed nested surfaces in the standard H-1 magnetic configuration (with no current in the helical winding and moderate vertical field) is clearly seen in Fig. 3. This configuration was obtained at ten radial positions of the electron gun, i.e., contains ten drift surfaces. Each measured drift surface contains up to 200 punctures suggesting fairly low attenuation of the electron beam as it travels around the torus at a low background gas pressure (typically

Downloaded 19 Aug 2003 to 150.203.2.60. Redistribution subject to AIP license or copyright, see http://ojps.aip.org/rsio/rsicr.jsp

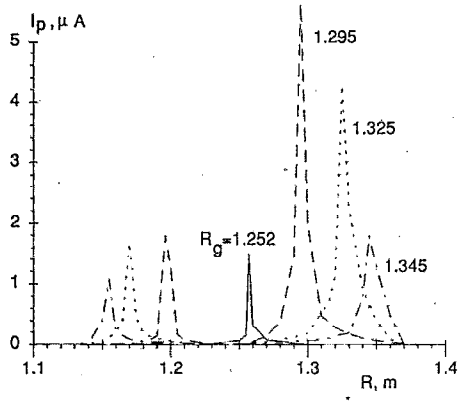

FIG. 4. Collector probe current as function of its position along the major radius ($z=0$) for different radial locations of the electron gun R_g.

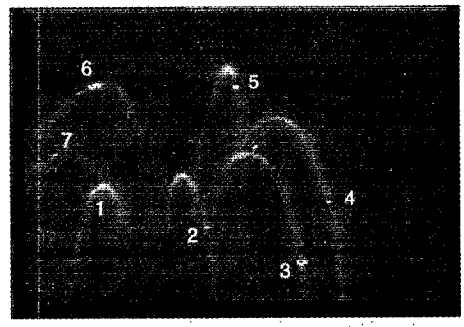

FIG. 5. Visible paths of the electron beam ($E=350$ eV) and superimposed punctures of the $\iota=8/7$ rational surface. Background pressure $p=4\times10^{-4}$ Torr in argon.

4×10^{-7} Torr). We tested experimentally whether the magnetic shear can lead to a poloidal spread of the electron beam and thus affect the width of the detected light spots on the target. For an emission current of the electron gun lower than 1 mA and the magnetic field $B=0.15$ T this effect was found to be negligible compared to the instrumental resolution (2–3 mm). The diameter of the electron beam is effectively defined by the 0.7 mm aperture of the electron gun with negligible spreading due to space charge. The size of the light spots is limited by the resolution of the CCD camera.

A collector probe is located in the $\phi=0°$ cross section of the torus to monitor the electron current in the field period not occupied by the electron gun and the fluorescent target. This can provide information on the breaking of the threefold toroidal symmetry of the heliac magnetic structure caused by the presence of an error field. The electric probe (a 4-mm-wide copper plate) insulated from ground is mounted on the coil support structure and is driven from the outside the vacuum tank very similarly to the electron gun. As the probe moves along the major radius of the machine, one can measure the electron current to the probe to obtain the position of the drift surfaces or the magnetic axis. Figure 4 demonstrates radial profiles of the electron current measured by the probe for four positions of the electron gun. Two narrow peaks are observed for each gun position except when the electron gun is on the magnetic axis, when only one peak is observed. In this case, the radial position of the magnetic axis found by the probe differs from that measured by the fluorescent target by 3 mm. The discrepancy between these measurements and a prediction of a computer model is 2 and 5 mm, respectively.

Measurements of the rotational transform are important to confirm the results of the computations. The images of the drift surfaces themselves contain no information on the rotational transform since the number of toroidal transits for each puncture of the electron beam in the poloidal plane are not known. The relative brightness of the spots can not be used in our experiment for ordering of the toroidal transits (as on the W7-AS stellarator[5]) because of the limited dynamical range of the CCD camera (8 bits). Instead, we use the visible paths of the electron beam to identify the number of toroidal transits corresponding to the successive light spots. For this purpose images of the beam paths are taken at much higher pressure than we use for the mapping. High quality drift surfaces are measured at $p=4\times10^{-7}$ Torr. Photographs of the beam paths are taken at $p=(0.8–2)\times10^{-4}$ Torr in argon. Up to ten toroidal transits can be clearly seen in this range of pressure and we are able to unambiguously order the visible paths of the electrons since the attenuation of the electron beam is high. By superimposing the image of the 3D visible paths on the untransformed 2D image of the drift surface the toroidal transit number can be identified for each of the light spots in the surface picture. Figure 5 presents the image of the electron paths with the $\iota=8/7$ rational surface superimposed. To limit the number of the detectable light spots on the drift surface to 10–15 the surfaces used for ι measurement are mapped at the higher than usual pressure ($p=5\times10^{-6}$ Torr). After ordering the light spots the image of the drift surface is transformed and the rotational transform is calculated as

$$\iota_m=\frac{1}{M}\sum_{j=1}^{M}\frac{\theta_j-\theta_{j-1}}{2\pi}, \tag{2}$$

where θ_j is a poloidal angle of the light spot corresponding to the jth toroidal transit. Shown in Fig. 6 are the computed and measured values of rotational transform in the standard mag-

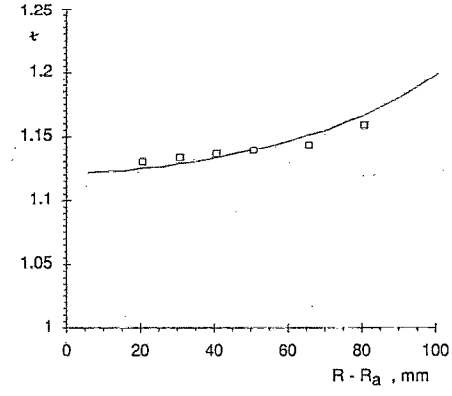

FIG. 6. Measured (squares) and computed (solid line) profile of rotational transform for the standard configuration. $R-R_0$ is a distance measured from magnetic axis along the major radius.

Downloaded 19 Aug 2003 to 150.203.2.60. Redistribution subject to AIP license or copyright, see http://ojps.aip.org/rsio/rsicr.jsp

netic configuration. We used $M=8$ toroidal transits to calculate ι for the data in Fig. 6. The discrepancy between the measured and computed values is about 0.8%. The accuracy of the ι measurement is about 1.5% (when $M=8$). This accuracy can be estimated if a rational surface is observed in the configuration,

$$\frac{\Delta\iota}{\iota}=\frac{\iota_r-\iota_m}{\iota_r}, \tag{3}$$

where $\iota_r=m/n$ is the exact value of the rotational transform at the rational surface.

IV. CONCLUSIONS

Magnetic mapping on the H-1 heliac has been performed using a directed electron beam and fluorescent target that combines the advantages of the fluorescent rod and the fluorescent mesh systems. Good spatial resolution (about 3 mm) and a high transparency of the apparatus resulted in high quality drift surface images. The existence of closed nested flux surfaces in H-1 has been confirmed, as has the threefold toroidal symmetry in the standard magnetic configuration. Measurements of the rotational transform using the visible electron beam to obtain the toroidal transit sequence are also in good agreement with the computed results.

ACKNOWLEDGMENT

The authors would like to thank S. M. Hamberger for his active support and useful discussions.

[1] S. M. Hamberger, B. D. Blackwell, L. E. Sharp, and D. B. Shenton, Fusion Technol. **17**, 123 (1990).

[2] J. F. Harris, J. L. Cantrell, T. C. Hender, B. A. Carreras, and R. N. Morris, Nucl. Fusion **25**, 623 (1985).

[3] F. S. B. Anderson, F. Middleton, R. J. Colchin, and D. Million, Rev. Sci. Instrum. **60**, 795 (1989).

[4] H. Hailer, J. Massig, F. Schuler, K. Schworer, and H. Zwicker, in *Proceedings of the 14th European Conference on Control Fusion and Plasma Physics*, Madrid, 1987 (European Physical Society, Geneva, 1987), Vol. 11D, Part 1, p. 423.

[5] R. Jaenicke, E. Ascasibar, P. Grigull, I. Lakicevic, A. Weller, M. Zippe, H. Hailer, and K. Schworer, Nucl. Fusion **33**, 687 (1993).

[6] T. Y. Tou, B. D. Blackwell, and L. E. Sharp, Rev. Sci. Instrum. **62**, 1149 (1991).

[7] G. J. Hartwell, R. F. Gandy, M. A. Henderson, J. D. Hanson, D. G. Swanson, and C. J. Bush, Rev. Sci. Instrum. **59**, 460 (1988).

[8] R. J. Colchin, F. S. B. Anderson, A. C. England, R. F. Gandy, J. H. Harris, M. A. Henderson, D. L. Hillis, R. R. Kindsfather, D. K. Lee, D. L. Million, M. Murakami, G. H. Neilson, M. J. Saltmarsh, and C. M. Simpson, Rev. Sci. Instrum. **60**, 2680 (1989).

Downloaded 19 Aug 2003 to 150.203.2.60. Redistribution subject to AIP license or copyright, see http://ojps.aip.org/rsio/rsicr.jsp